Robust Rician noise estimation for MR images.

Pierrick Coupé, José V. Manjón, Elias Gedamu, Douglas L. Arnold, Montserrat Robles, D Louis Collins

Robust Rician Noise Estimation for MR Images

Pierrick Coupé [a,*], José V. Manjón [b], Elias Gedamu [a], Douglas Arnold [a], Montserrat Robles [b], D. Louis Collins [a].

[a] *McConnell Brain Imaging Centre, Montréal Neurological Institute, McGill University 3801, University Street, Montréal, Canada H3A 2B4 bDivision of Neurosurgery, McGill University, Montréal, Canada*

[b] *Instituto de Aplicaciones de las Tecnologías de la Información y de las Comunicaciones Avanzadas (ITACA), Universidad Politécnica de Valencia, Camino de Vera s/n, 46022 Valencia, Spain.*

Abstract

In this paper, a new object-based method to estimate noise in magnitude MR images is proposed. The main advantage of this object-based method is its robustness to background artefacts such as ghosting. The proposed method is based on the adaptation of the Median Absolute Deviation (MAD) estimator in the wavelet domain for Rician noise. The MAD is a robust and efficient estimator initially proposed to estimate Gaussian noise. In this work, the adaptation of MAD operator for Rician noise is performed by using only the wavelet coefficients corresponding to the object and by correcting the estimation with an iterative scheme based on the SNR of the image. During the evaluation, a comparison of the proposed method with several state-of-the-art methods is performed. A quantitative validation on synthetic phantom with and without artefacts is presented. A new validation framework is proposed to perform quantitative validation on real data. The impact of the accuracy of noise estimation on the performance of a denoising filter is also studied. The results obtained on synthetic images show the accuracy and the robustness of the proposed method. Within the validation on real data, the proposed method obtained very competitive results compared to the methods under study.

* Corresponding author.
Email address: pierrick.coupe@gmail.com (Pierrick Coupé).

1 Introduction

In MR image analysis, the estimation of the noise level in an image is a mandatory step that must be addressed to assess the quality of the analysis and the consistency of the image processing technique. The noise variance is also an important measure for many image processing techniques such as denoising or registration. Furthermore, procedures that employ statistical analysis techniques, such as functional MR imaging or voxel-based morphometry, often based their conclusions on assumptions about the underlying noise characteristics [35].

Usually, the real and imaginary parts of the MR complex raw data are considered corrupted by white additive Gaussian noise, where the noise variance is assumed to be the same in both parts (real and imaginary) [19,20]. By taking the magnitude of the complex data, the noise is transformed into Rician noise [2,19–21,37]. Noise in magnitude MR images can be well modeled by a Rician distribution when computed from a single complex raw data [8,11,20,21], but may not model the noise correctly for other types of acquisitions. For example, in multichannel signal acquisition reconstructed by the sum of squares of the complex images, the noise distribution can be described by noncentral χ-distribution [8,11,12]. Moreover, in case of parallel imaging (i.e. multichannel signal acquisition with parallel reconstruction), the noise amplitude varies according to the spatial localization in the image and can follow Rician or χ-distribution according to the reconstruction technique [11–13].

In this paper, we consider only the cases where the Rician model can be used. Conventionally, the Rician noise is *i*) described by Rayleigh distribution in the background [2,19,20,37] (i.e. the signal of air in the background is considered to be zero), and *ii*) approximated by Gaussian noise in the foreground when Signal Noise Ratio (SNR) is high enough (> 3 [29]). These models for background and foreground noise distribution have been used in the majority of noise estimation methods [2,36,37]. However, the Rayleigh model of the background can fail when ghosting artefacts are present (i.e. non-zero signal) [37], and the Gaussian approximation of foreground is no longer valid for images with low SNR [37].

In the past, measuring the Rician noise variance has been done by using one or more MR images. A relatively simple approach to estimate the Rician noise variance is to use the difference between two matched images of the same object [28]. Although the technique is simple to implement, its efficiency relies heavily on the correct alignment of the two images. Therefore, techniques that use a single image may be preferred. The first methods using a single image were based on manual selection of uniform signal or non-signal regions [20,37]. However such techniques are time consuming and have a high intra and inter

user variability.

Naturally, some automatic techniques have been proposed [2, 36–38]. Usually, these methods use the histogram of the background and some properties of the Rayleigh distribution. A common manner to measure the Rician noise variance in magnitude MR images with large enough background areas is to estimate it from the mode of the histogram [36–38]. Recently, a new noise Rician variance estimation method based on maximum likelihood (ML) estimation from a partial histogram was presented by Sijbers [37]. More recently, Aja *et al.* [2] presented a set of new methods for noise estimation based on local statistics that are able to estimate the noise variance from the background but also from the imaged object in a very simple and efficient manner.

In this paper, an adaptation of the Median Absolute Deviation (MAD) estimator in the wavelet domain is proposed for Rician noise. This robust and efficient estimator has been proposed by Donoho [14] for Gaussian noise and since has been widely used in image processing. We propose to adapt this operator for Rician noise by using only the wavelet coefficients corresponding to the object and then iteratively correcting the MAD estimation with an analytical scheme based on the SNR of the image [21]. The second aim of this paper is to compare some of the previously mentioned state-of-the-art methods against our method using synthetic data (with and without artefacts) and clinical datasets.

The structure of this paper is as follows: Section 2 gives a brief overview of the theoretical aspects of the noise properties in MR images. Section 3 presents the proposed Rician MAD estimator. Section 4 describes the state-of-the-art methods used during the comparison. Section 5 presents the synthetic data experiments, Section 6 the real data experiments and the section 7 the study on denoising performance. Finally, Section 8 discusses the applicability of the proposed method and future extensions of the proposed work.

2 Noise in MR images

As mentioned in the introduction, when MR images are computed using the magnitude of a single complex raw data, the distribution of noise can be modeled with a Rician distribution [11, 12, 19, 20, 37]:

$$p(m) = \frac{m}{\sigma_n^2} exp(-\frac{m^2 + A^2}{2\sigma_n^2}) I_0(\frac{Am}{\sigma_n^2}). \quad (1)$$

where σ_n is the standard deviation (STD) of Gaussian noise in the complex domain, A is the amplitude of the signal without noise, m is the value in the magnitude image and I_0 is the zeroth order modified Bessel function [31]. This

model is used by the majority of the noise estimation methods [2,36,37]. Most of these methods can be classified as: *i*) methods that use background areas to estimate the noise variance and *ii*) methods that use the image object itself.

- **For the background-based methods**, where the signal is usually considered as zero in background (i.e. SNR = 0), the Rician distribution is a Rayleigh distribution [16,37]:

$$p(m) = \frac{m}{\sigma_n^2} exp(-\frac{m^2}{2\sigma_n^2}). \tag{2}$$

  Based on the properties of the Rayleigh distribution, the mean $\bar{m}_b$ and the variance σ_b^2 of the noise in the background can be related to σ_n:

$$\overline{m}_b = \sqrt{\frac{\pi}{2}}\sigma_n \tag{3}$$

$$\sigma_b^2 = \frac{4-\pi}{2}\sigma_n^2 \tag{4}$$

  The assumption that SNR = 0 in the background may not be valid in the presence of ghosting artefacts [37], while the Rayleigh distribution assumption can be corrupted by using reconstruction filters [11,12,24], by the suppression of the signal by the scanner [12,24] or by zero-padding in the Fourier domain [24]. Finally, the noise level in the background may not be representative of the noise level inside the tissue [11,24].
- **For the object-based methods with high SNR** (i.e. SNR > 3) [19, 29], the Rician distribution can be well approximated using a Gaussian distribution:

$$p(m) \approx \frac{1}{2\pi\sigma_n^2} exp(-\frac{(m^2 - \sqrt{A^2+\sigma_n^2})^2}{2\sigma_n^2}). \tag{5}$$

  This approximation enables us to use all the classical methods proposed for Gaussian noise estimation. Nevertheless, for low SNR, this approximation is no longer valid [19,29,37].

3 Proposed method

In order to relax the assumptions performed by background-based methods (i.e. no signal in the background) and the object-based methods (Gaussian noise approximation), we propose an adaptation of the MAD estimator in wavelet domain [14,15] for Rician noise.

3.1 MAD estimator

The wavelet transformation is usually used to obtain a space-frequency representation of images. By using the usual notation for 3D wavelet decomposition: LLL denotes the low sub-band containing the feature information whereas LHH, LHL, LLH, HLL, HLH, HHL and HHH denote the high sub-bands containing the detailed information. The highest sub-band HHH is essentially composed of coefficients that correspond to the noise [14, 15]. The capacity of the wavelet transforms to distinguish between noise and structure has been used in denoising methods to remove or reduce the coefficients corresponding to the noise components over the detailed sub-bands [14, 15]. The fact that the highest sub-band HHH is mainly composed of the coefficients corresponding to the noise has been used by Donoho [14, 15] to propose a robust estimation of noise variance. Based on the MAD estimator, this method enables the estimation of the noise variance in presence of Gaussian noise:

$$\hat{\sigma} = \frac{median(|y_i|)}{0.6745} \tag{6}$$

where y_i are the wavelet coefficients of the HHH sub-band and $\hat{\sigma}$ the estimation of noise in magnitude image. The noise in magnitude image σ will be called "magnitude noise" as in [21] in the following. As long as the y_i coefficients corresponding to the object are considered and the SNR is high enough, the Gaussian approximation of Rician noise leads to $\hat{\sigma}_n = \hat{\sigma}$.

3.2 Rician adaptation

To obtain an unbiased estimation of σ_n for all the SNR values, we propose to use the correction procedure introduced by Koay *et al* in [21]. This analytical correction is based on an iterative estimation of the SNR in presence of Rician noise. In our case, the estimation $\hat{\sigma}$, obtained using the MAD estimator on the object, is used to initialize the procedure:

$$\hat{\sigma}_n = \sqrt{\hat{\sigma}^2/\xi(\theta)} \tag{7}$$

where θ is the SNR value and ξ is the correction factor, which is expressed as:

$$\xi(\theta) = 2 + \theta^2 - \frac{\pi}{8} \times exp\left(-\frac{\theta^2}{2}\right)\left((2+\theta^2)I_0\left(\frac{\theta^2}{4}\right) + \theta^2 I_1\left(\frac{\theta^2}{4}\right)\right)^2 \tag{8}$$

where I_1 is the first order modified Bessel function. The correction factor is iteratively applied until convergence of the procedure or when a given number of iterations t is achieved. The distance $|\theta_t - \theta_{t-1}|$ can be used as stop criterion.

The resulting iterative correction scheme can be written as:

$$\theta_t = \sqrt{\xi(\theta_{t-1})\left(1 + \frac{\overline{m}_o}{\hat{\sigma}}\right) - 2} \tag{9}$$

where $\overline{m}_o$ is the mean signal of the object and $\hat{\sigma}$ the first estimation from MAD estimator. The correction factor $\xi(\theta_t)$ from the last iteration is finally used in Eq. 7.

3.3 Object extraction

The STD estimation of the "magnitude noise", $\hat{\sigma}$, is solely based on the wavelet coefficients corresponding to the object. To extract the object we take advantage of the wavelet transform. Since the noise information is mainly contained in the highest sub-bands, the LLL sub-band contains a less noisy version of the image which can be used to facilitate the segmentation procedure. At the first level of decomposition, the size of LLL and HHH are identical. Thus, at this level of decomposition, we proposed to segment the object in the LLL sub-band and to use the obtained mask to extract the y_i coefficients corresponding to the object in the HHH sub-band. The segmentation is performed using a simple K-means (k=2) classification [25].

For an image with a low level of noise, the MAD estimation tends to be spoiled since the HHH sub-band is mainly composed of information corresponding to the high gradient (HG) areas (i.e. edges) of the image. To further increase the accuracy of the estimation at low noise levels, voxels with the highest local gradient are excluded from the estimation (i.e. removed from the segmented mask). Accordingly, we eliminate all those voxels whose the local gradient magnitude is higher than the median local gradient magnitude in the LLL sub-band. A comparison of the MAD estimation of the "magnitude noise" STD over the segmented mask with and without HG is proposed in the experiment section.

The use of more elaborate wavelet decomposition such as Dual-Tree (DTWT) or Complex Dual-Tree (DTCWT) [34] can improve wavelet-based image processing [27]. In our method we use classical wavelet transform (WT) [26] as implemented in `http://taco.poly.edu/WaveletSoftware/standard3D.html`. A comparison of the MAD estimator applied on WT and on DTWT is provided in the experiments section.

4 Evaluated Methods

In this section, we provide a brief description of the five methods used during the experiments. The original papers can be referred to for more details.

4.1 Background-based methods

The first is a method proposed by Sijbers *et al.* [37] which is based on the maximum likelihood estimation principle over a partial histogram H_p. The ML estimate is found by maximizing the likelihood function L with respect to the standard deviation of noise σ_n using the first K bins of the histogram with a Rayleigh distribution assumption for the background:

$$\hat{\sigma}_n = \arg\max_{\sigma_n} L(\sigma_n, H_p) \tag{10}$$

The optimal number of bins, K, of the partial histogram is automatically estimated from the bias and the variance of the estimator $\hat{\sigma}_n$.

The two other background estimators were recently proposed by Aja *et al.* [2]. These estimators use the robust properties of the image's local statistics (local means and local variances). The distributions of the local means $\hat{\mu}$ and the local variances $\hat{v}$ are used to estimate the variances of noise under the Rayleigh distribution assumption of the background. Using the properties of the Rayleigh distribution given in Eq. 3 and Eq. 4, Aja *et al.* propose to estimate the noise standard deviation as follows:

$$\hat{\sigma}_n = \sqrt{\frac{2}{\pi}} mode(\hat{\mu}) \tag{11}$$

with local means and:.

$$\hat{\sigma}_n = \sqrt{\left(\frac{4-\pi}{2}\right)\left(\frac{N}{N-1}\right) mode(\hat{v})} \tag{12}$$

with local variances, where N is is the number of data points used to calculate the local variances.

4.2 Object-based methods

The two object-based methods are the MAD estimator and the estimator based on local variances $\hat{v}$ proposed by Aja *et al.* in [2]. This estimator has

been proposed when no background is available in the image and is based on a Gaussian approximation of the noise within the object:

$$\hat{\sigma}_n = \sqrt{mode(\hat{v})} \tag{13}$$

5 Experiments on Synthetic data

In this section, the description of the material used such as the Rician noise simulation or the ghosting artefacts construction is first described. The estimation of the STD of "magnitude noise" is then studied. To achieve this, the capability of the proposed method based on MAD estimator to estimate σ over the HHH subband is studied on a constant image and on a T1-w phantom. A validation framework is finally proposed to study the accuracy and the robustness of the STD estimation of Rician noise σ_n provided by the different methods.

5.1 Material

5.1.1 Phantom data

To evaluate the different methods, synthetic T1-weighted MR data from the Brainweb database [6,7,23] was corrupted with different levels of Rician noise (2 to 15%). In this paper, 2% of noise is equivalent to $\mathcal{N}(0, \nu\frac{2}{100})$, where ν is set to 255, the maximum intensity of the original 8bit encoded image. All the synthetic data are converted into 32bit encoded images before adding noise, in order to avoid quantification artefact during experiment on phantom [13]. The Rician noise was built from white Gaussian noise in the complex domain:

- $I_r = A + \eta_1$, $\eta_1 \backsim \mathcal{N}(0, \sigma_n)$
- $I_i = \eta_2$, $\eta_2 \backsim \mathcal{N}(0, \sigma_n)$

where A is the noise free "ground truth" from Brainweb, I_r is the real component, I_i is the imaginary component, and σ_n is the standard deviation of the added white Gaussian noise. The noisy image is computed as:

$$m = \sqrt{I_r^2 + I_i^2} \tag{14}$$

As shown in [2], the size of the background has an impact on the accuracy of the background-based methods. Smaller backgrounds lead to more difficult estimations. In order to perform a fair comparison, zero padding of the Brain-

web volume of $181 \times 217 \times 181$ voxels was perfromed to obtain a volume of $256 \times 217 \times 256$ voxels.

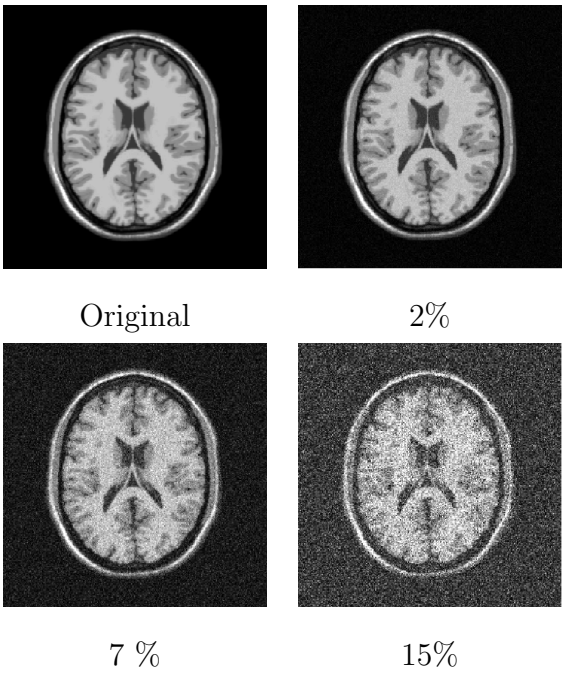

Fig. 1. Simulation of Rician noise for different levels.

5.1.2 Intensity inhomogeneities

MR images are normally affected by intensity inhomogeneities produced during the image acquisition process. Such inhomogeneities can affect the noise measurement process. To investigate the effect of such inhomogeneities on the performance of the different noise estimation methods, the bias field in in the Brainweb simulator was applied to the data. For our experiments, a 20% inhomogeneity level was chosen. As the bias field only affects the imaged object, the background methods should not be impacted by this artefact.

5.1.3 Ghosting artefacts

Ghosting artefacts were implemented by using a repeated filtered version of the original image. First, the image is low-pass filtered with two gaussian kernels of different size ($3 \times 3 \times 3$ and $5 \times 5 \times 5$). Then, the absolute difference of the two filtered images is added to the original image with a half field of view offset (see Fig. 2).

5.1.4 Compared methods

During our experiments on σ_n estimation, we compared the following methods:

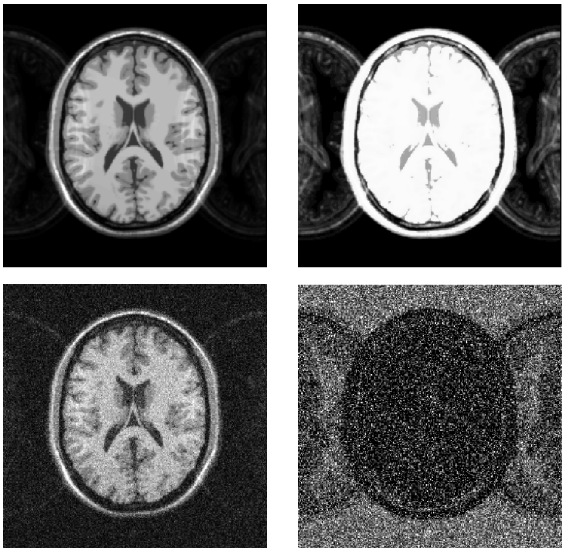

Fig. 2. Top. Right: Simulated ghosting artefacts on brainweb with 20% inhomogeneity. Left: The same image with saturation of the contrast to highlight the ghosting artefacts. Bottom. Right: The same image with 7% of Rician noise. Left: The added Rician noise.

- a background-based method proposed by Sijbers [37]; denoted as "ML" and described in section 4.1. The Sijbers method was applied using a histogram with 1000 bins.
- two background-based methods based on local statistics [2]; denoted as LMB for the Local Means in Background and LVB for Local Variances in Background. These methods are described in section 4.1. The size of the local neighborhoods and the number of bins were $5 \times 5 \times 5$ voxels and 1000 bins respectively.
- an object-based method based on local variances [2]; denoted as LVO for Local Variances in Object, and described in section 4.2. For this method, a local neighborhood of $3 \times 3 \times 3$ voxels was used. In contrast to the background, the object has smaller homogeneous areas. As a result, we have reduced the spatial extends of our local neighborhood.
- the classical MAD estimator estimated on the object [14]. The object was segmented in the wavelet domain without removing high gradient areas.
- the proposed robust MAD for Rician noise estimated on the object and denoted as RMAD (see section 3).

5.2 Validation of σ estimation

5.2.1 On a constant image

First, the capability of the MAD estimator to estimate the STD of "magnitude noise" in an easy case (i.e. without structure information within the highest

wavelet subband) has been studied. To achieve this, an image with constant intensity c close to the mean intensity of tissues included in the mask (i.e. $c = 100$) has been created. Different levels of Rician noise were then applied from 2% to 15%. The true value of σ and the estimation provided by the MAD estimation $\hat{\sigma}$ was compared. Equation 15 was used to compute the STD of the applied "magnitude noise" σ. The experiment was repeated ten times, each with a new instantiation of noise, for each noise level.

$$\sigma = \sqrt{\sigma_n^2 . \xi(\theta)} \tag{15}$$

The SNR θ is simply computed as $\theta = c/\sigma_n$.

Figure 3 shows the result of the experiment. For all the levels of noise, the error in MAD estimation is inferior to 0.25%. This experiment shows that the MAD estimator is able to robustly estimate the STD of "magnitude noise" for a large range of noise levels. Moreover, this experiment shows that the coefficients in HHH subband are able to properly describe the noise STD.

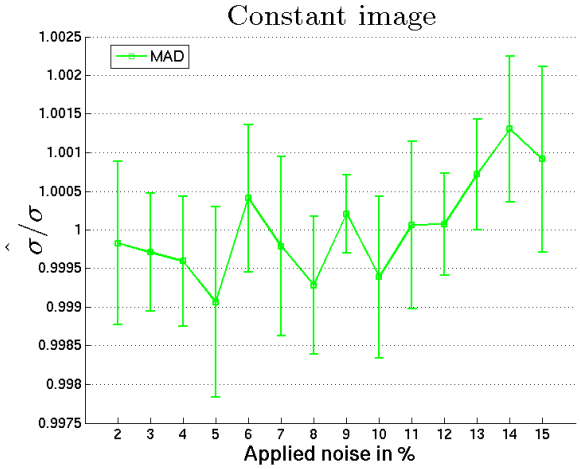

Fig. 3. Ratio between the standard deviation of "magnitude noise" σ and the estimation given by MAD on a constant image.

5.2.2 On T1-w phantom

The second experiment has been designed to show: a) the impact of the highest gradient (HG) removal on the MAD estimator, b) the capability of the proposed approach (segmentation in wavelet domain with K-means and MAD estimation over the object wavelet coefficients) to robustly estimate the STD of "magnitude noise", c) the impact between using classical separable wavelet transform and the dual tree wavelet transform (DTWT), and d) the ability of coefficient in HHH subband to fully-describe the "magnitude noise" STD in a realistic situation.

As in the previous experiment, we compared the true value of σ and the

estimation provided by the MAD estimator: $\hat{\sigma}$. In this case, the SNR was computed by using the mask (provided by K-means segmentation in wavelet domain on the noisy image) on the original noise-free image in order to get the true mean signal value μ. The SNR θ was computed as $\theta = \mu/\sigma_n$. Finally, Equation 15 has been used to obtain σ. The experiment has been repeated ten times, each with a new instantiation of noise, for each noise level.

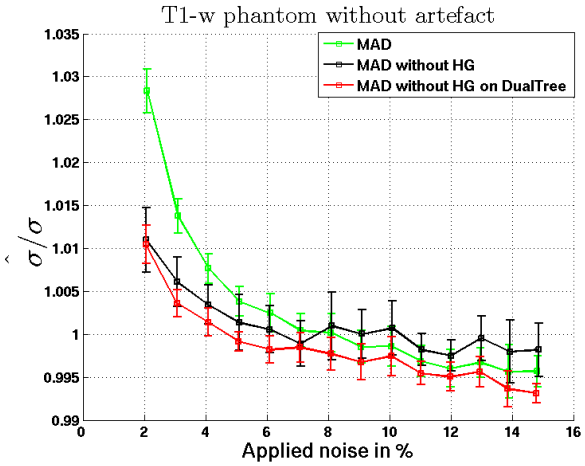

Fig. 4. Ratio between the standard deviation of "magnitude noise" σ and the estimation given by MAD estimator on a T1-w phantom image.

Figure 4 shows the result of the comparison between MAD estimation, MAD estimation without HG areas and MAD estimation without HG on Dual Tree decomposition. As previously mentioned, at low levels of noise, the MAD estimator tends to overestimate the noise level. However, HG removal divides the error by a factor 3 at 2% noise level. Moreover, if the MAD estimation without HG on DTWT provided more stable (smaller variance) than the MAD estimation without HG on WT, the accuracy of the estimation is not better over all the noise levels. Due to the additional computational burden and memory requirement needed by DTWT compared to WT, especially in 3D, we have chosen to use classical WT in the proposed method.

5.3 Validation of σ_n estimation

To study the accuracy of the evaluated methods to estimate the Rician noise STD σ_n, the ratio between the estimated standard deviation $\hat{\sigma}_n$ and the applied standard deviation σ_n is computed for all the levels of noise. Moreover, the Mean Absolute Error over all the levels of noise is also used. The absolute error for a given level of noise is computed as:

$$error = |1 - \frac{\sigma_n}{\hat{\sigma}_n}| \tag{16}$$

All the experiments were repeated 10 times, each with a new instantiation of noise, for each noise level and the average results are presented.

5.3.1 "Ideal case"

Figure 5 (on top) shows the experimental results on the phantom without artefacts. For this "ideal case", all the methods provide a satisfying result, especially the methods based on local statistics of the background (LMB and LVB) and the proposed RMAD. These estimators demonstrated small mean absolute errors ($< 1\%$). The LMB method provided the best result for this experiment.

Compared to the MAD estimator, the ability of the RMAD method to correctly estimate the higher levels of noise (i.e. where the Gaussian assumption failed) can be attributed to the SNR based correction factor. Moreover, the RMAD provided better estimations of the noise at low level by removing the high gradients before the MAD computation.

As expected, for high levels of noise, the Gaussian assumption used by MAD and LVO failed and these methods provided an underestimation. For low levels of noise, the LVO method produced an overestimation of σ_n since the local variances contain edges information, thus artificially increasing the variance of noise. The LVO method also has the largest variability of estimation at all levels of noise.

5.3.2 Impact of Ghosting artefact

Figure 5 (on middle) shows the results on the phantom with ghosting artefacts. The wavelet-based methods produced similar results compared to the results obtained in "ideal case". The LVO method seems to be negatively affected due to the extra edge information added in the image. As expected, the most impacted methods are the background-based methods. In fact, the assumption of zero signal in the background is spoiled by ghosting. All these methods tend to overestimate the noise level, especially the ML method. The LMB method still obtained very good results. Finally, the RMAD method obtained the best result.

5.3.3 Impact of inhomogeneities

Figure 5 (on bottom) shows the results on the phantom with ghosting artefacts and inhomogeneities. Contrary to an expected error increase from the object-based approaches, the inhomogeneities did not impact the performance of these methods. The robust methods used by these approaches (wavelet and

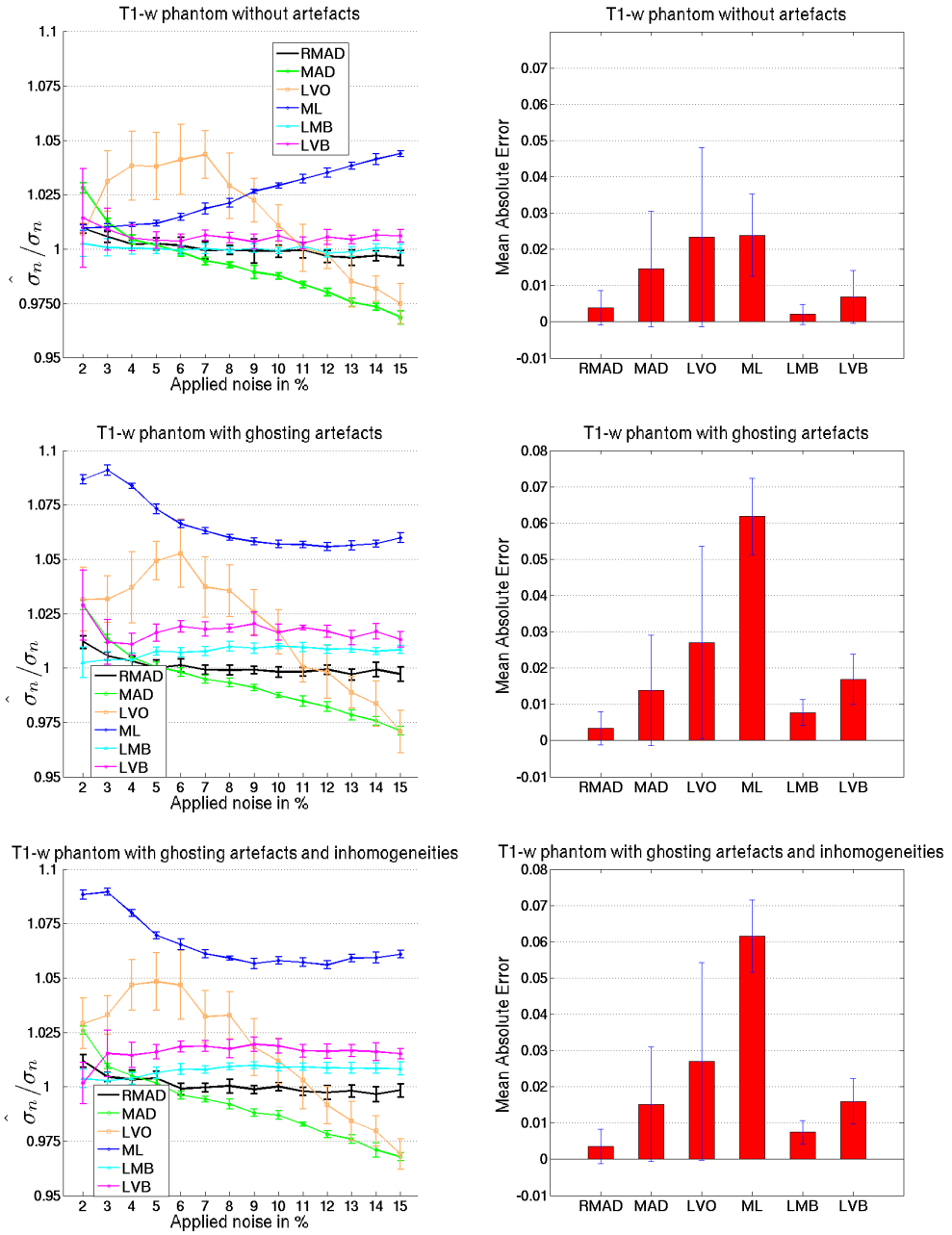

Fig. 5. Left: results of the compared methods for all levels of noise on the synthetic image. Right: mean absolute error over all noise levels.

local variance) seem to protect them against this kind of artefact.

6 Experiments on Clinical data

In this section, we proposed a new evaluation framework on real data. The validation of noise estimation methods in clinical context is a challenging prob-

lem due to the absence of "ground truth". In our experiments, we proposed to use a bronze standard to quantify the performance of each method on two datasets composed of single-channel (1CH) T1-w MR data from two different sites.

6.1 Material

6.1.1 Data

The data analyzed was acquired in the context of a multicenter clinical trial. All subjects gave written consent and the studies were approved by their respective institutions. The first dataset from site 1 was composed of 23 T1-w MR volumes of $256 \times 256 \times 56$ voxels. These data were acquired with a 1.5T Genesis Signa GE Medical system and an 1CH head coil. The parameters of the sequence were: TR = 30ms, TE = 9ms, FOV 250 mm and bandwidth 122 kHz. The second dataset from site 2 was composed of 42 T1-w MR volumes of $256 \times 256 \times 60$ voxels. These data were acquired with a 1.5T Genesis Signa GE Medical system and an 1CH head coil. The parameters of the sequence were: TR = 34ms, TE = 9ms, FOV = 250 mm and the bandwidth = 122 kHz. All the images are 16bit encoded. Examples of data with and without artefacts are presented in Fig. 6.

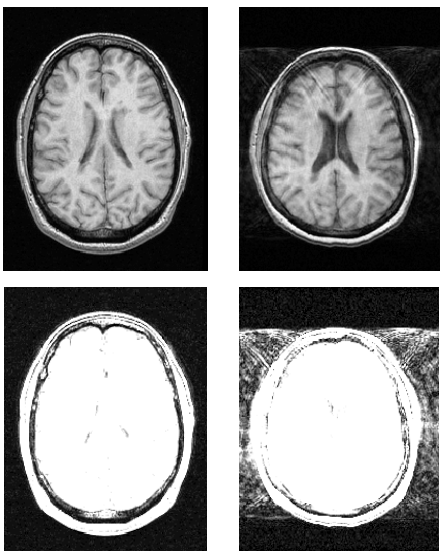

Fig. 6. Left: data without ghosting artefacts. Right: data with ghosting artefacts. Saturation of the contrast is used to highlight the ghosting artefacts.

6.1.2 Background extraction

In order to estimate the noise level in the real images, we used a region-based approach that is similar to the manual selection procedure usually used in the clinical environment.

Moreover, in order to perform a fair comparison, we used a background-based method to build our bronze standard. Given the large number of data volumes in the study, and the fact that we wanted to minimize intra- and inter-rater variability in noise estimation, we opted to use an automatic quality control (aQC) software tool [17] to identify the background region of interest (ROI). Experiments in [17] show that this method is robust, accurate, and highly correlated with manual methods.

The aQC is a series of pipelined tests that are designed to assess the quality of MR brain images. Most of the tests are based on the statistical analysis of selected regions of interest (see Fig. 7), three of which are associated with noise regions (region 1: four corners that surround the head, region 2: anterior to the head, region 3: posterior to the head, and region 4: regions lateral to the head). To determine the noise level, we used the region anterior to the head (region 2). In [17], it has been shown that this region contains less artefacts, thus provides a robust estimation of the background noise. The other two regions were susceptible to flow artifacts based on the position of the head and phase encode direction. This occurs primarily in the region posterior to the head.

All the ROIs that are used by the aQC reside in the standard MNI coordinate space. Accordingly, for each subject, the selected ROI is registered from MNI-space to the image's native coordinate space. Once the ROI is aligned to the image of interest d, its background $\hat{m}_b(d)$ is extracted. By the way, we extracted the original background values avoiding interpolation of image intensities, and prevents the modification of noise characteristic [32].

Noise Region 1: Four corners surrounding | Noise Region 2 and 3: Anterior and posterior | Noise Region 4: Lateral

Fig. 7. Noise regions of interest obtained with automated quality control software tool [17].

6.1.3 Bronze standard

The estimation of a Bronze standard on real images is not an easy task since the ground truth is unknown. In our study, we have chosen to use the assumption that the noise level for a given sequence on the same scanner should be constant. Based on this idea, the noise regions extracted from the backgrounds of MR images are used to estimated an average level of noise over all the data from a same site. To estimate this average level of noise, the properties of the second-order moment of a Rician distribution are used. For a random variable m following a Rician distribution this moment can be written as:

$$\mathbb{E}(m^2) = A^2 + 2\sigma_n^2 \tag{17}$$

By using the assumption of SNR $= 0$ in the background:

$$\sigma_n = \sqrt{\frac{\overline{\mathbb{E}(m_b^2)}}{2}} \tag{18}$$

Finally, for a given site, the Bronze standard can be computed from the mean of the squared values extracted from backgrounds of all the data d:.

$$\hat{\sigma}_n = \sqrt{\frac{\overline{\hat{M}_b^2}}{2}}, \hat{M}_b^2 = (\hat{m}_b^2(1), ..., \hat{m}_b^2(D)) \tag{19}$$

where $\hat{m}_b^2(d)$ is the vector containing the squared value of noise extracted from the background of data d and $\hat{M}_b^2$ is the concatenation of the squared signal from all the data. This procedure is performed independently for each site. The region anterior to the head (region 2) tends to minimize the presence of background artefacts in the extracted background. The visual inspection of the $\hat{m}_b^2(d)$ has confirmed that the used regions were minimally impacted by ghosting. Moreover, by computing the mean value over a large number of datasets, the impact of residual non visible artefacts is drastically reduced. By the way, the extracted backgrounds may not totally free of ghosting, but the impact on the bronze standard is minimized.

Based on the same approach, the estimation of the noise level for a given data d is obtained with the region-based (RB) method by using the mean of the squared values extracted from the background of d:

$$\hat{\sigma}_n(d) = \sqrt{\frac{\overline{\hat{m}_b^2(d)}}{2}} \tag{20}$$

In this case, the noise estimation is less robust than the estimation used for the bronze standard since only one background region sample is involved.

Fig. 8 (on top) shows the results obtained for site 1. For all the data, RMAD method provided a consistant estimation of the noise relative to the Bronze standard (small error) in a robust manner (small variance of error). The stability of the proposed method leads to a smaller error than the region-based method that was used to build the bronze standard. As assessed by experiments on synthetic phantom, the MAD estimator computed on the object tends to underestimate the noise level whereas the LVO method leads to an overestimation of the noise level. The LVB method appear to follow the MAD estimation and the RMAD estimation according to the data. The LMB method estimated in the background is a robust and stable estimator but leads to a slight underestimation. Finally, the ML method provided a good mean absolute error but was accomplished with a high variability.

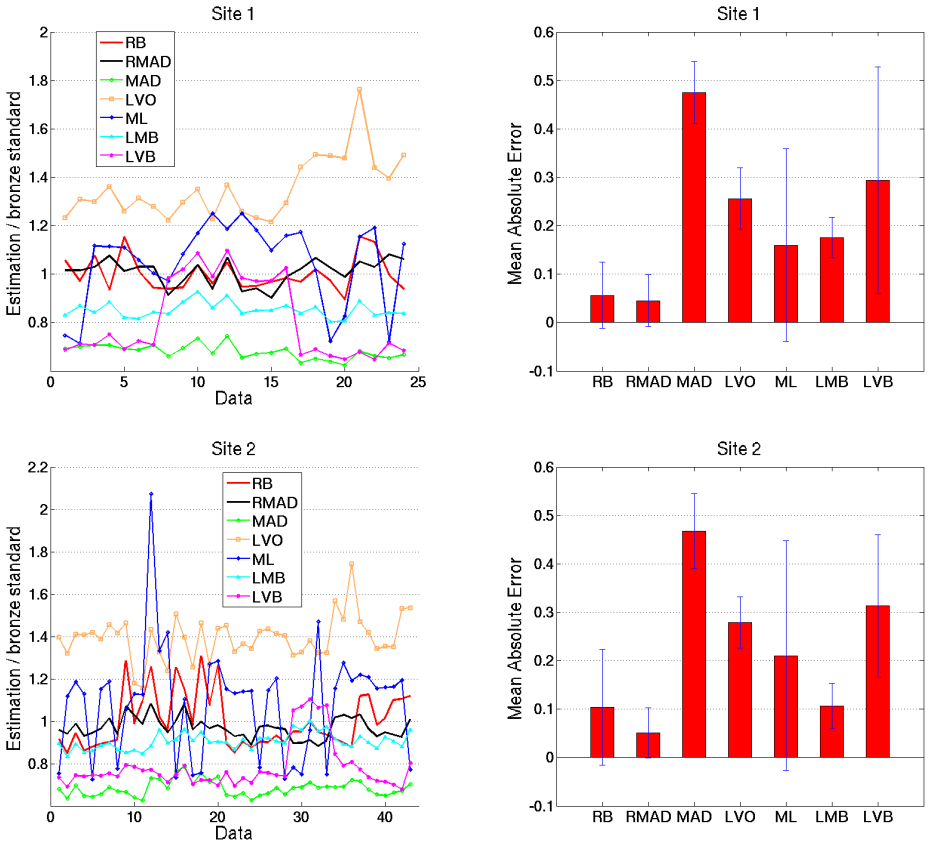

Fig. 8. Left: results of the compared methods for all the data. Right: mean absolute error over all the data.

Fig. 8 (on bottom) shows the results obtained for site 2. The remarks made for site 1 apply to this site as well. It should be noted that the LMB method yielded better results for this site and maintained a small mean absolute. This method provided similar result to the region-based method used for the Bronze

standard estimation but with a smaller variance. For both sites, the RMAD method obtained the best results.

7 Experiment on denoising performance

As said in the introduction, one application of the STD noise estimation is denoising. In the literature, many approaches have been proposed for MRI denoising [1, 3, 5, 9, 10, 18, 22, 29, 30, 33, 40]. In this last experiment, we propose to study the impact of noise estimation accuracy on denoising performance of the 3D NonLocal-Means filter described in [10] with the Rician adaptation proposed in [39]. In our framework, the noise estimation accuracy impacts a) the filtering parameter (smoothing parameter) (see [10] for details) as well as b) the intensity bias correction (see [39] for details). Like the other experiments presented in this paper, the denoising algorithm has been applied ten times for each noise level from 2% up to 15% on the T1-w phantom corrupted with ghosting and inhomogeneity. The quality criterion used was the difference between the Peak Signal to Noise Ratio (PSNR) obtained with the estimation $\hat{\sigma}_n$ provided by each method (i.e. PSNR($\hat{\sigma}_n$)) and the PSNR obtained with the truth σ_n (i.e. PSNR(σ_n)). The PSNR was computed as:

$$PSNR = 20 \log_{10} \frac{255}{RMSE} \tag{21}$$

where RMSE denotes the root mean square error estimated between the ground truth and the denoised image. The PSNR values were estimated only in the region of interest (cerebral tissues) obtained by removing the background (i.e. the label 0 of the discrete model in Brainweb). This has been done in order to avoid artificial increasing of PSNR due to overclamping in background.

Figures 9 and 10 show the results of the experiment. In a large majority of noise levels, the proposed method demonstrates a better denoising than the other evaluated methods. The LMB method proposed by Aja *et al.* also obtained good results. In terms of mean absolute error, the proposed RMAD obtained the best denoising performance over all the noise levels. Visually, the denoised images obtained with the evaluated methods look very similar, indicating that the bias intensity correction is more impacted by noise estimation inaccuracy than the denoising process. In case of quantitative MR study, where the true value of intensity is required, our method has great potential.

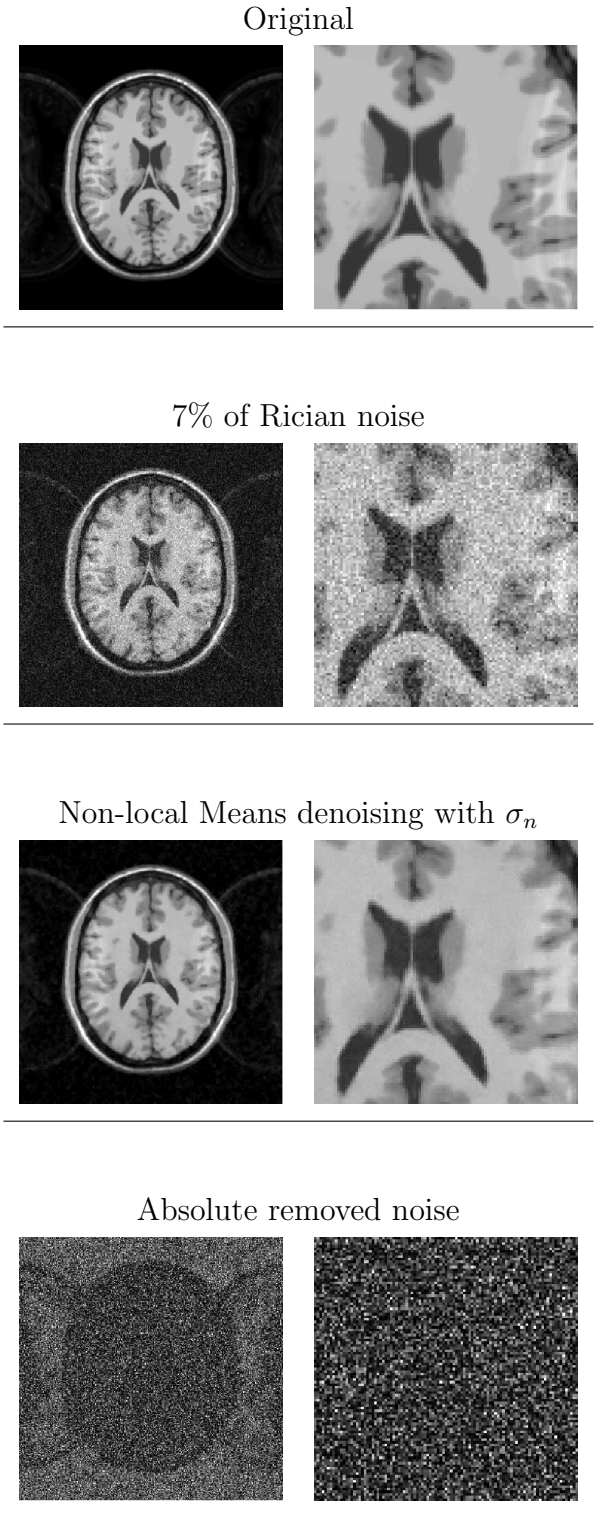

Fig. 9. From top to bottom: original image with ghosting and inhomogeneity, the same image with 7% of Rician noise, the result of the denoising with the true value σ_n, the absolute removed noise.

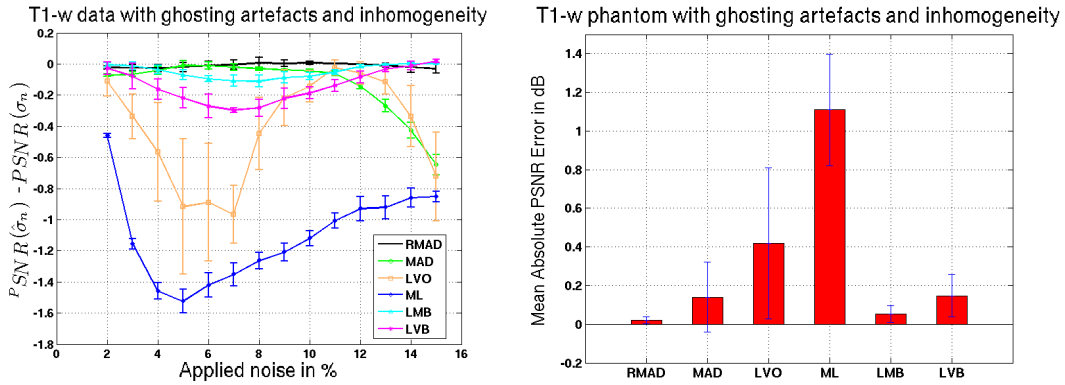

Fig. 10. Result of the denoising experiment. Left: difference in dB between the PSNR obtained with the estimation provided by automatic methods $\hat{\sigma}_n$ and the PSNR obtain with the truth σ_n. Right: mean absolute difference in dB between PSNR(σ_n) and PSNR($\hat{\sigma}_n$).

8 Discussion

In this paper, a new method based on the robust MAD estimator for Rician noise has been proposed and several state-of-the-art methods for Rician noise estimation in MR image have been compared.

Experiments on synthetic data have shown that for the "ideal case" (i.e. when an image does not contain any artefacts), the method proposed by Aja *et al.* based on the mode of the distribution of local means is the best option showing no systematic errors in the estimation. When ghosting artefacts are added, the proposed RMAD estimator outperforms all the compared methods. As expected for high level of noise, the methods based on Gaussian approximation (object-based MAD and LVO methods) underestimate the noise level. Moreover, the object-based method that uses the local variances tend to overestimate the level of noise for low level of noise since the assumption of constant area in the object is not satisfied. The ML method proposed by Sijbers *et al.* tends to overestimate the noise variance as the noise power increases or when ghosting artefacts are added. This is probably due to the overlap of background and the imaged object distributions in the image histogram.

Experiments on real data have shown that for the two sites studied, the proposed RMAD method obtained the best result in terms of accuracy and robustness. The background-based methods had the highest variability except the LMB method which provided a robust noise estimation. These results show that the variance of background in real data is spoiled by artefacts. The MAD estimation lead to a systematic underestimation of the noise level due to Gaussian approximation. As observed for synthetic experiments, the LVO method that use the local variances on object overestimates the noise level.

Experiment on denoising have shown that the proposed method is able to obtain better denoising results than other noise estimation methods thanks to its high accuracy in the presence of artefacts.

In addition to obtaining very competitive results in "ideal" situations and better results in presence of ghosting compared to state-of-the-art background methods, our method enables the estimation of noise over the techniques compared in many other situations found in clinical routine. In fact, contrary to classical background approaches, the proposed approach can be applied to situations where no background is present such as fetal imaging or images where the background is artificially set to zero by the scanner [11] (see Fig. 11). Moreover, since the proposed method does not performed Gaussian approximation, our approach is able to deal with high level of noise such as noise in HARDI DTI data (see Fig. 11).

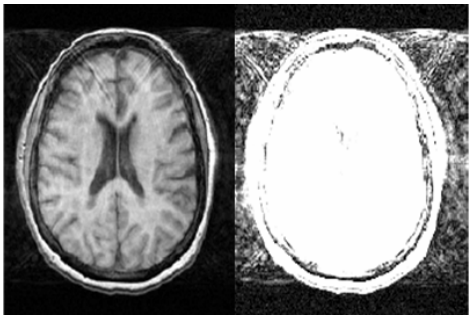

Ghosting

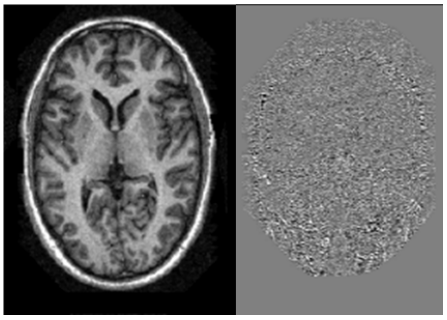

Background set to zero by MR scanner

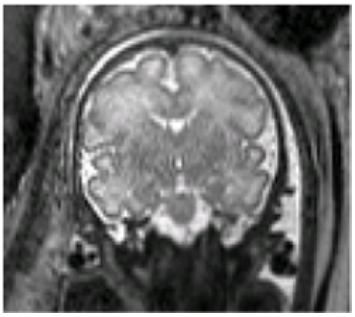

No background available

(e.g. Fetal imaging)

High level of noise

(e.g. HARDI DTI data)

Fig. 11. Situations where our method can be used while classical methods cannot or failed. *MRI without background courtesy of Dr. G. Garcia-Marti, fetal image courtesy of Dr. Limperopoulos, DTI data courtesy of Pr. Pike.*

In future work, the proposed approach should be adapted to multi-channels signal acquisitions (noncentral χ-distribution) [4, 21] and for images with non stationary noise such as those attributed to parallel imaging (i.e. GRAPPA or SENSE). The multi-channels signal acquisitions are becoming more often

used during clinical acquisitions and the investigation of methods dedicated to these images should be further investigated. Moreover, the new sequences of acquisition can produce images with correlated noise due to interpolation in K-space. The adaptation of the proposed method to correlated noise should be also investigated as done for denoising [1, 5].

Acknowledgements

We are grateful to Dr. Sijbers and Dr. Aja for providing the source code of their respective Rician noise estimation methods and for their useful comments. We thank the reviewers for their valuable comments which have improved this paper. We also thank Dr Levesque for the fruitful discussions on MR image acquisition. We want to thank NeuroRx research for providing the clinical MR data used during experiment. This work has been partially supported by a grant from the Canadian Institutes of Health Research (MOP-84360), by the Canadian grant Industry Cda (CECR)-Gevas-OE016, and by the Spanish Health Institute Carlos III through the RETICS Combiomed, RD07/0067/2001.

References

[1] J. Aelterman, B. Goossens, A. Pizurica, and W. Philips. Removal of correlated rician noise in magnetic resonance imaging. In *16th European Signal Processing Conference (EUSIPCO 2008)*, 2008.

[2] S. Aja-Fernandez, C. Alberola-Lopez, and C. F. Westin. Noise and signal estimation in magnitude MRI and Rician distributed images: a LMMSE approach. *IEEE transactions on image processing*, 17(8):1383–1398, August 2008.

[3] S. Aja-Fernandez, M. Niethammer, M. Kubicki, M. E. Shenton, and C. F. Westin. Restoration of dwi data using a rician lmmse estimator. *Medical Imaging, IEEE Transactions on*, 27(10):1389–1403, 2008.

[4] S. Aja-Fernández, A. Tristán-Vega, and C. Alberola-López. Noise estimation in single- and multiple-coil magnetic resonance data based on statistical models. *Magnetic Resonance Imaging*, 27(10):1397 – 1409, 2009.

[5] M. E. Alexander, R. Baumgartner, C. Windischberger, E. Moser, and R. L. Somorjai. Wavelet domain de-noising of time-courses in mr image sequences. *Magnetic Resonance Imaging*, 18(9):1129 – 1134, 2000.

[6] C. A. Cocosco, V. Kollokian, R. K. Kwan, G. B. Pike, and A. C. Evans. Brainweb: Online interface to a 3D MRI simulated brain database. In *NeuroImage*, page 425, 1997.

[7] D.L. Collins, A.P. Zijdenbos, V. Kollokian, J.G. Sled, N.J. Kabani, C.J. Holmes, and A.C. Evans. Design and construction of a realistic digital brain phantom. *IEEE Transactions on Medical Imaging*, 17(3):463–468, 1998.

[8] C.D. Constantinides, E. Atalar, and E. McVeigh. Signal-to-noise measurements in magnitude images from nmr phased arrays. *Engineering in Medicine and Biology Society, 1997. Proceedings of the 19th Annual International Conference of the IEEE*, 1:456–459 vol.1, Oct-2 Nov 1997.

[9] P. Coupé, P. Hellier, S. Prima, C. Kervrann, and C. Barillot. 3D wavelet subbands mixing for image denoising. *Journal of Biomedical Imaging*, 2008(3):1–11, 2008.

[10] P. Coupé, P. Yger, S. Prima, P. Hellier, C. Kervrann, and C. Barillot. An Optimized Blockwise NonLocal Means Denoising Filter for 3-D Magnetic Resonance Images. *IEEE Transactions on Medical Imaging*, 27(4):425–441, April 2008.

[11] O. Dietrich, J. G. Raya, S. B. Reeder, M. Ingrisch, M. F. Reiser, and S. O. Schoenberg. Influence of multichannel combination, parallel imaging and other reconstruction techniques on mri noise characteristics. *Magnetic Resonance Imaging*, 26(6):754 – 762, 2008.

[12] O. Dietrich, J. G. Raya, S. B. Reeder, M. F. Reiser, and S. O. Schoenberg. Measurement of signal-to-noise ratios in mr images: Influence of multichannel coils, parallel imaging, and reconstruction filters. *Journal of Magnetic Resonance Imaging*, 26(2):375–385, 2007.

[13] O. Dietrich, J. G. Raya, and M. F. Reiser. Magnetic resonance noise measurements and signal-quantization effects at very low noise levels. *Magnetic Resonance in Medicine*, 60(6):1477–1487, 2008.

[14] D.L. Donoho. De-noising by Soft-Thresholding. *IEEE Transactions on Information Theory*, 41(3):613–627, 1995.

[15] D.L. Donoho and I.M. Johnstone. Ideal spatial adaptation by wavelet shrinkage. *Biometrika*, 81(3):425–455, 1994.

[16] W. A. Edelstein, P. A. Bottomley, and L. M. Pfeifer. A signal-to-noise calibration procedure for NMR imaging systems. *Medical Physics*, 11:180–185, March 1984.

[17] E. L. Gedamu, D. L. Collins, and D. L. Arnold. Automated quality control of brain MR images. *Journal of Magnetic Resonance Imaging*, 28(2):308–319, August 2008.

[18] G. Gerig, R. Kikinis, O. Kübler, and F.A. Jolesz. Nonlinear anisotropic filtering of MRI data. *IEEE Transactions on Medical Imaging*, 11(2):221–232, June 1992.

[19] H. Gudbjartsson and S. Patz. The Rician distribution of noisy MRI data. *Magnetic Resonance in Medicine*, 34:910–914, 1995.

[20] R. M. Henkelman. Measurement of signal intensities in the presence of noise in MR images. *Medical Physics*, 12(2):232–233, 1985.

[21] C. G. Koay and P. J. Basser. Analytically exact correction scheme for signal extraction from noisy magnitude MR signals. *Journal of Magnetic Resonance*, 179(2):317–322, April 2006.

[22] Karl Krissian and Santiago Aja-Fernández. Noise-driven anisotropic diffusion filtering of mri. *IEEE transactions on image processing : a publication of the IEEE Signal Processing Society*, 18(10):2265–2274, October 2009.

[23] R. K. Kwan, A. C. Evans, and G. B. Pike. MRI simulation-based evaluation of image-processing and classification methods. *IEEE Trans Med Imaging*, 18(11):1085–1097, November 1999.

[24] B. Landman, P.-L. Bazin, and J. Prince. Diffusion Tensor Estimation by Maximizing Rician Likelihood. *Computer Vision, 2007. ICCV 2007. IEEE 11th International Conference on*, pages 1–8, Oct. 2007.

[25] J. B. MacQueen. Some methods for classification and analysis of multivariate observations. In L. M. Le Cam and J. Neyman, editors, *Proc. of the fifth Berkeley Symposium on Mathematical Statistics and Probability*, volume 1, pages 281–297. University of California Press, 1967.

[26] Stéphane Mallat. A theory for multiresolution signal decomposition: The wavelet representation. *IEEE Trans. Pattern Anal. Mach. Intell.*, 11(7):674–693, 1989.

[27] Yves Meyer. *Oscillating Patterns in Image Processing and Nonlinear Evolution Equations: The Fifteenth Dean Jacqueline B. Lewis Memorial Lectures*. American Mathematical Society, Boston, MA, USA, 2001.

[28] B. W. Murphy, P. L. Carson, J. H. Ellis, Y. T. Zhang, R. J. Hyde, and T. L. Chenevert. Signal-to-noise measures for magnetic resonance imagers. *Magnetic Resonance Imaging*, 11(3):425 – 428, 1993.

[29] R. Nowak. Wavelet-based rician noise removal for magnetic resonance imaging. *IEEE Transactions on Image Processing*, 8(10):1408–1419, October 1999.

[30] A. Pizurica, W. Philips, I. Lemahieu, and M. Acheroy. A versatile wavelet domain noise filtration technique for medical imaging. *IEEE Trans. Medical Imaging*, 22:323–331, 2003.

[31] S. O. Rice. Mathematical Analysis of Random Noise. *Bell Systems Tech. J.*, 23:282–332, 1944.

[32] G. K. Rohde, A. S. Barnett, P. J. Basser, and C. Pierpaoli. Estimating intensity variance due to noise in registered images: applications to diffusion tensor mri. *NeuroImage*, 26(3):673–684, July 2005.

[33] A. Samsonov and C. R. Johnson. Noise-adaptive nonlinear diffusion filtering of MR images with spatially varying noise levels. *Magnetic Resonance in Medicine*, 52(4):798–806, 2004.

[34] I.W. Selesnick, R.G. Baraniuk, and N.C. Kingsbury. The dual-tree complex wavelet transform. *Signal Processing Magazine, IEEE*, 22(6):123–151, Nov. 2005.

[35] L. Sendur, V. Maxim, B. Whitcher, and E. Bullmore. Multiple hypothesis mapping of functional mri data in orthogonal and complex wavelet domains. *Signal Processing, IEEE Transactions on*, 53(9):3413–3426, Sept. 2005.

[36] J. Sijbers, A.J. den Dekker, J. Van Audekerke, M. Verhoye, and D. Van Dyck. Estimation of the noise in magnitude MR images. *Magnetic Resonance Imaging*, 16(1):87–90, 1998.

[37] J. Sijbers, D. Poot, A. J. den Dekker, and W. Pintjens. Automatic estimation of the noise variance from the histogram of a magnetic resonance image. *Physics in Medicine and Biology*, 52(5):1335–1348, 2007.

[38] G. M. van Kempen and L. J. van Vliet. Influence of background estimation on the superresolution properties of nonlinear image restoration algorithms. In *Society of Photo-Optical Instrumentation Engineers (SPIE) Conference Series*, volume 3605, pages 179–189, May 1999.

[39] N. Wiest-Daesslé, S. Prima, P. Coupé, S.P. Morrissey, and C. Barillot. Rician noise removal by non-local means filtering for low signal-to-noise ratio mri: Applications to DT-MRI. In *11th International Conference on Medical Image Computing and Computer-Assisted Intervention, MICCAI'2008*, New York, USA, September 2008.

[40] J.C. Wood and K.M. Johnson. Wavelet packet denoising of magnetic resonance images: importance of Rician noise at low SNR. *Magn Reson Med*, 41(3):631–635, March 1999.